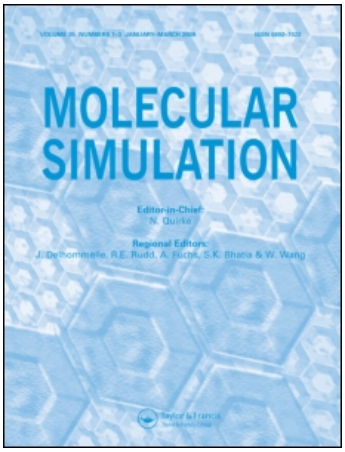

Molecular Simulation
Publication details, including instructions for authors and subscription information:
http://www.informaworld.com/smpp/title~content=t713644482

Thermal behaviour of Pd clusters inside carbon nanotubes: insights into the cluster-size, tube-size and metal-tube interaction effects

Daojian Cheng[a]; Jianhui Lan[b]
[a] Laboratoire Physique des Solides Irradiés et des Nanostructures, CP234, Faculté des Sciences, Université Libre de Bruxelles, Bruxelles, Belgium [b] Division of Molecular and Materials Simulation, Key Lab for Nanomaterials, Ministry of Education, Beijing University of Chemical Technology, Beijing, P.R. China

Online publication date: 15 October 2010

To cite this Article Cheng, Daojian and Lan, Jianhui(2010) 'Thermal behaviour of Pd clusters inside carbon nanotubes: insights into the cluster-size, tube-size and metal-tube interaction effects', Molecular Simulation, 36: 10, 805 — 814
To link to this Article: DOI: 10.1080/08927021003762720
URL: http://dx.doi.org/10.1080/08927021003762720

Molecular Simulation
Vol. 36, No. 10, September 2010, 805–814

Taylor & Francis
Taylor & Francis Group

Thermal behaviour of Pd clusters inside carbon nanotubes: insights into the cluster-size, tube-size and metal–tube interaction effects

Daojian Cheng[a]* and Jianhui Lan[b]

[a]*Laboratoire Physique des Solides Irradiés et des Nanostructures, CP234, Faculté des Sciences, Université Libre de Bruxelles, Bd du Triomphe, Bruxelles B1050, Belgium;* [b]*Division of Molecular and Materials Simulation, Key Lab for Nanomaterials, Ministry of Education, Beijing University of Chemical Technology, Beijing 100029, P.R. China*

(*Received 18 December 2009; final version received 9 March 2010*)

Molecular dynamics simulations were used to investigate the cluster-size, tube-size and metal–tube interaction effects on the melting of Pd clusters encapsulated inside carbon nanotubes (CNTs). The second moment approximation to the tight-binding potential was used to model Pd–Pd metal–metal interaction and the Tersoff potential was used for C–C interactions. Pd–C interaction was modelled by the typical weak van der Waals Lennard-Jones (VDW-LJ) potential to understand the cluster-size and tube-size effects on the thermal behaviour of supported Pd clusters. Linear decrease in cluster melting point with the inverse in cluster diameter is predicted for the CNT containing Pd clusters, well known as Pawlow's law. It is also found that the melting temperature of the supported Pd cluster is much lower than that of free one, and the rearrangement and transformation of the cluster at higher temperatures before melting are responsible for this lowering. In this case, the downward shift is independent of the CNT diameter for the same Pd cluster. In addition, the Pd–C interaction was redefined to assess the metal–tube interaction effect on the thermal evolution of the CNT-containing Pd clusters by fitting to first-principle calculations. Using the fitted strong density functional theory-Morse Pd–C potential, deformation for the CNT and structural transformation from the icosahedral to the stacked for the Pd cluster inside the CNT are found, which is not shown by using the VDW-LJ potential.

Keywords: molecular dynamics; melting; metal cluster; carbon nanotubes

1. Introduction

Recent experimental and theoretical advances in metal clusters have attracted widespread interest [1,2]. From the point of view of applications, metal clusters are promising nanomaterials in catalytic [3], magnetic [4] and optical fields [5]. In addition, interest in metal clusters arises because their properties and structures are size dependent [6,7]. On the other hand, carbon nanotubes (CNTs) are provided with a well-defined tubular morphology with inner hollow cavities, making them the ideal support for metal clusters [8]. Several studies have shown that metal/CNT encapsulates exhibit various fascinating new properties and are suitable for applications as, for instance, magnetic recording media [9,10], biological sensors [11] or nanocatalysts [12–15]. Most often, transition metal clusters are dispersed on the outer CNT surface in experiments [9,11,13,15], since the confinement of transition metal clusters inside CNTs is still a challenge [12,14]. However, the introduction of transition metal clusters inside CNTs may improve the performances of the materials because of the combination of short-channel effects and the extraordinary physical and chemical properties of CNTs [12,14].

We are interested in CNT-supported Pd clusters since Pd is widely used as a high-performance sensor [16,17] and is a catalyst for hydrogenation reactions [12,14]. Recent literature results [17,18] showed that Pd clusters located outside CNT exhibit high sensitivity and selectivity towards hydrogen, and are able to sense hydrogen with excellent mechanical flexibility and durability at near room temperature. Lu et al. [16] found that CNTs loaded with Pd clusters can be used for the detection of methane ranging from 6 to 100 ppm in air at room temperature. On the other hand, Pd clusters encapsulated inside CNTs exhibit excellent activity, selectivity and stability for the hydrogenation of cinnamaldehyde into hydrocinnamaldehyde at low temperatures, compared with those observed using traditional catalysts [14]. Zhang et al. [12] found that Pd clusters in CNTs exhibit higher activity in liquid-phase benzene hydrogenation than other supports such as Y zeolite and activated carbon.

Considering the high cost of both CNTs and palladium, it is necessary to optimise the structure and properties of Pd clusters in CNTs, in order to get better efficiency for sensors or catalysts at low cost. To achieve such a goal, it is necessary to study both the cluster-size and tube-size effects on the properties of Pd clusters encapsulated in CNTs, and to identify the role of the interaction of metal clusters with the CNTs. Unfortunately, the measure

*Corresponding author. Email: dcheng@ulb.ac.be

ISSN 0892-7022 print/ISSN 1029-0435 online

DOI: 10.1080/08927021003762720
http://www.informaworld.com

of cluster size, tube size and metal–tube interaction effects is experimentally difficult. Therefore, it is necessary to use molecular simulation or other theoretical methods to address this topic.

Molecular simulation, based on semi-empirical potentials, is suitable to study the structures, properties and thermodynamics of metal clusters encapsulated inside CNTs. Cheng et al. [19] studied the thermal evolution of a platinum cluster encapsulated in CNTs, using a Monte Carlo method, and found that the tube size affects significantly the melting-like structural transformation of the icosahedral clusters. Arcidiacono et al. [20] investigated the solidification of gold clusters inside CNTs using molecular dynamics (MD) and found that the solidification temperature of the supported cluster is higher than that of the corresponding unsupported cluster. Moreover, Morrow and Striolo [21,22] studied the morphology and mobility of platinum nanoparticles of various sizes supported by CNTs. They found that the structures and properties of the Pt clusters depend on the support morphology. However, the theoretical studies on the Pd clusters encapsulated inside CNTs are still scarce.

The typical weak van der Waals Lennard-Jones (VDW-LJ) potential was used in most of the previous investigations, including all of those simulations mentioned above. These VDW-LJ potential parameters were commonly derived from MD simulations of pure metals and carbon supports using the Lorentz–Berthelot mixing rules [23,24]. Nevertheless, the metal–carbon interaction could be fitted to first-principle calculations. Recent *ab initio* results by Acharya et al. [25] showed that the metal–carbon interaction is much stronger than those previously used. By using the potential of Acharya et al., Morrow and Striolo [26] studied the structure of platinum nanoparticles supported on graphite and various bundles of CNTs. They found that the Pt–C interaction has a great effect on the structures of the supported Pt clusters. In addition, Chen and Kawazoe [27] studied the interaction between a single Pt atom and a CNT using density functional theory (DFT), and strong binding energies were found for the Pt atom on the outer wall of a small radius nanotube.

In the present work, we use the MD method to investigate the thermal behaviour of the Pd clusters encapsulated inside CNTs. The typical VDW-LJ potential is used to understand the effects of the metal cluster size and the size of the CNT on the melting of the Pd clusters. Another Pd–C interaction is fitted to first-principle calculations so as to address the metal–tube interaction effect on the thermal evolution of CNT-containing Pd clusters.

2. Computational details

MD was used to study the melting of free and CNT-supported Pd clusters using the DL_POLY version 2.19 codes [28]. MD simulations were performed with a constant number of atoms N with a nearly zero fluctuating pressure P. The temperature was maintained constant by the Berendsen thermostat [29] with a relaxation time of 0.4 ps. Newton's equations of motion were integrated using the Verlet leapfrog algorithm and the integration time step was set to 0.5 fs. For the melting of the free Pd clusters, no periodic boundary conditions were applied. However, one periodic boundary condition was applied along the nanotube axis for studying Pd clusters inside CNTs. At each temperature, the first 100 ps were used for the atomic structure relaxation, and the next 200 ps were used for statistical averaging. The Pd clusters inside CNTs were first equilibrated in the 0–50 K interval. Then, simulations were performed in a series of temperature conditions starting from 50 K with 50 K temperature increments. Near the melting point, the increment was reduced to 10 K.

Five armchair (n, n) single-walled nanotubes with the chirality of (15, 15), (20, 20), (25, 25), (30, 30) and (35, 35) were adopted in this work. The Pd clusters of interest possess closed shell icosahedral structures. Accordingly, clusters with sizes of 55, 147, 309 and 561 were used. Figure 1(a) depicts the initial configurations of the Pd clusters inside a (30, 30) CNT. Figure 1(b) gives the initial snapshots of the Pd_{147} cluster inside (15, 15), (20, 20), (25, 25), (30, 30) and (35, 35) CNTs. In all cases, the centre of mass of the clusters was initially located at the centre of the CNT.

Three interactions have to be distinguished in this work. The second moment approximation to the tight-binding (TB-SMA) potential [30] was used to model the interaction between Pd and Pd. In this potential, the total Pd–Pd interaction energy, $E_{\mathrm{Pd-Pd}}$, can be expressed as

$$E_{\mathrm{Pd-Pd}} = \sum_{i}^{N} \left(\sum_{j \neq i}^{N} A\, \mathrm{e}^{-p(r_{ij}/r_0 - 1)} - \sqrt{\sum_{j \neq i}^{N} \xi^2\, \mathrm{e}^{-2q(r_{ij}/r_0 - 1)}} \right), \tag{1}$$

where r_{ij} is the distance between atoms i and j in the cluster, r_0 is the equilibrium nearest-neighbour distance in the pure metals and N is the number of metal atoms. The TB-SMA potential parameters for the Pd–Pd interaction are taken from Ref. [30], as shown in Table 1.

The C–C interactions were modelled using a many-body empirical Tersoff potential since it describes the C–C bonds in CNTs reliably [31]. It should be mentioned that the Tersoff potential has already been employed for the theoretical study of metal systems encapsulated into CNTs successfully [32,33].

Since the metal–carbon interaction is presently still not well known until now, two different Pd–C potentials were used to compare the outcome. One is a weak interaction model using the 12-6 Lennard-Jones (VDW-LJ) potential

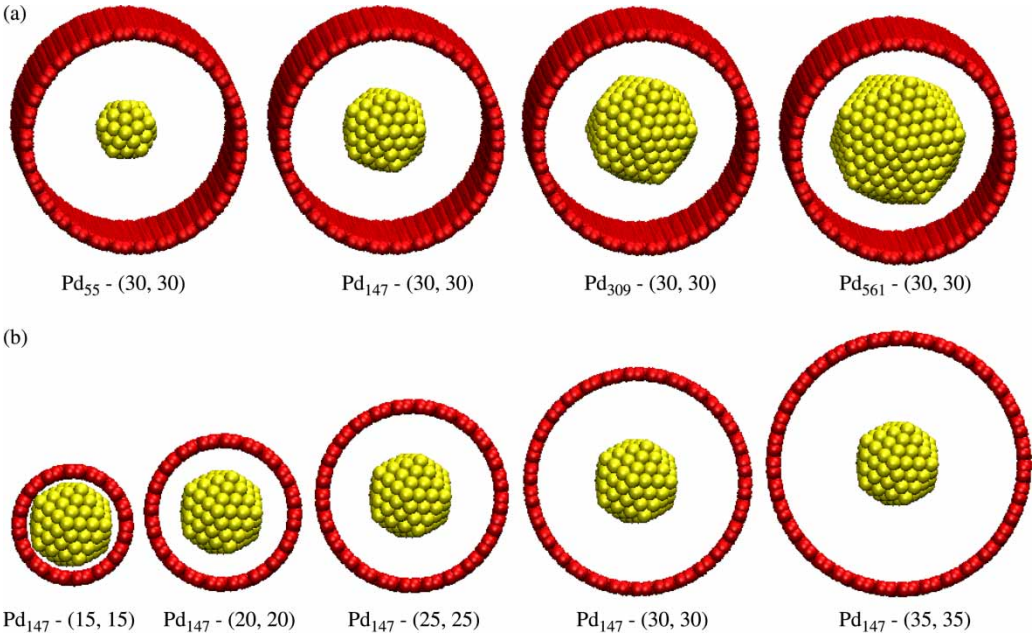

Figure 1. The initial configurations of (a) the Pd clusters with the sizes of 55, 147, 309 and 561 inside a (30, 30) CNT and (b) the Pd_{147} cluster inside (15, 15), (20, 20), (25, 25), (30, 30) and (35, 35) CNTs.

function. The potential parameters were derived from the data of pure metals and carbon supports using Lorentz–Berthelot mixing rules [23,24,34], as shown in Table 1. It should be mentioned that the VDW-LJ potential was used to understand the effects of the metal cluster size and the size of the CNT on the melting of the Pd clusters. On the other hand, a Morse-type potential fitted to the first-principle calculation was proposed so as to understand the metal–tube interaction effect on the thermal evolution of CNT-containing Pd clusters.

The first-principle calculations used for fitting the atom–atom interaction potential of Pd–C were performed in the framework of DFT with the Gaussian 03 program package [35]. The cluster model method was used in the first-principle calculation, and a large curved graphite-like sheet was adopted to represent the CNT adsorbent. Similar cluster models for CNTs were used in Refs [36–38].

Table 1. Parameters of the TB-SMA potential for the Pd–Pd interaction the 12-6 Lennard-Jones (VDW-LJ) potential for the Pd–C interaction and the Morse (DFT-Morse) potential by fitting for the Pd–C interaction.

TB-SMA potential for Pd–Pd		VDW-LJ potential for Pd–C		DFT-Morse potential for Pd–C	
A (eV)	0.1746	ε (eV)	0.0335	E_0 (eV)	0.1132
ξ (eV)	1.718	σ (Å)	2.926	r_0 (Å)	2.73
p	10.867			k	1.56
q	3.742				
r_0 (Å)	2.7485				

Figure 2 shows a schematic diagram of the cluster model used in this work for the first-principle calculation of the (15, 15) CNT. It is found in Figure 2 that 22 framework carbon atoms are included in this model. All the calculations in this paper were carried out with the PW91 exchange-correlation function [39].

On the inner wall of CNT surface, there are three typical adsorption sites: on top, bridge and hollow. Our results show that the hollow site is the most favourable adsorption one for a single Pd atom. Therefore, the

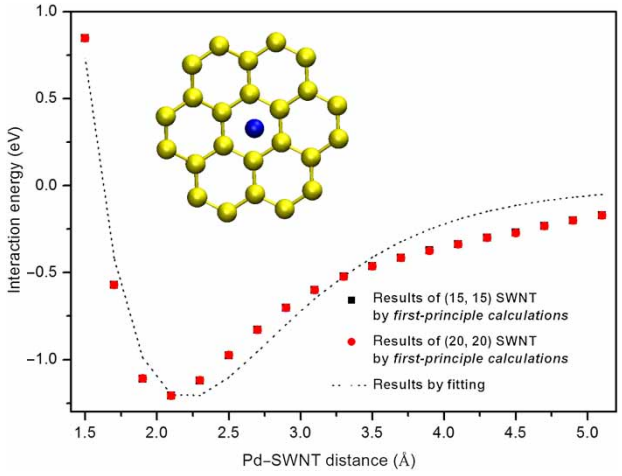

Figure 2. The fitted Pt–C potential energy curve, compared with the points calculated by the first-principle calculations. Sketch in the inner panel represents the CNT cluster model with a single Pd atom at the hollow site.

potential energy curve at the hollow site was used to derive the Pd–C atom–atom interaction in this work. Figure 2 shows the potential energy curve of Pd interaction with the inner walls of (15, 15) and (20, 20) CNT surfaces at the hollow site. The Pd–C atom–atom interaction was then parameterised by fitting the first-principle calculation results for the Pd atom on the graphite-like sheet including 22 framework carbon atoms. The fitted analytical form is based on a Morse potential (DFT-Morse) as follows:

$$E_{\mathrm{Pd-C}} = E_0\left[\{1 - \exp(-k(r_{ij} - r_0))\}^2 - 1\right], \qquad (2)$$

where r_{ij} is the distance between Pd atom and the inner wall of the tube surface in units of Å. In the fitting process, the Pd–carbon surface interactions are calculated by the summation of all the Pd–C atom–atom interactions. The parameters E_0, r_0 and k are given in Table 1. Figure 2 gives the fitted dependencies, compared with the discrete potential energies derived from the first-principle calculations. It should be mentioned that the potential energy curves of the Pd–C atom–atom interaction obtained by the first-principle calculations are nearly the same for the (15, 15) and (20, 20) CNTs, as shown in Figure 2. We thus used the same parameters to model the DFT-Morse Pd–C atom–atom interaction for the Pd clusters inside different CNTs. It is acknowledged that much more DFT calculations are necessary in order to improve and verify the Pd–C atom–atom interaction.

3. Results and discussion

We identify melting from the caloric curve of the Pd subsystem and the corresponding heat capacity C_v per atom. For the heat capacity, the following relationship is used:

$$C_v = \frac{\left(\langle E^2\rangle - \langle E\rangle^2\right)}{nk_{\mathrm{B}}T^2}, \qquad (3)$$

where E is the potential energy, k_{B} is the Boltzmann constant, n is the total number of the atoms in the cluster and T is the temperature. In addition, we used two indicators to analyse the melting processes, including the deformation parameter $\varepsilon_{\mathrm{def}}$ [40] and the bond-order parameter (BOP) method [41,42]. Deformation parameter $\varepsilon_{\mathrm{def}}$ represents a type of quadrupole deformation, and can be used to model the shape evolution during the melting. Its definition can be found elsewhere in Refs [40,43]. BOPs can capture the symmetry of bond orientations regardless of the bond length, which is useful to analyse the structural changes during the melting as well as to distinguish the atoms whether they are solid or liquid. Definitions of the BOPs and their standard values for a number of structures can be found elsewhere in References [34,41,43].

In Figure 3(a), an example is shown of the caloric curve and the heat capacity C_v per atom with respect to the temperature for the free Pd_{561} cluster. The temperature corresponding to the maximum peak value in the heat capacity C_v is in good agreement with the step jump in the caloric curve, and a melting temperature of about 910 K is predicted. Figure 3(b) gives the Pd caloric curve and the corresponding temperature dependence of C_v for the Pd_{561} cluster, encapsulated inside a (30, 30) CNT. In this case, a step jump in the caloric curve is found to be in agreement with the sharp peak in the corresponding heat capacity C_v per atom. Then, the melting point of the Pd_{561} cluster encapsulated inside a (30, 30) CNT is estimated to be 820 K.

In Figure 3(c), we give the temperature dependences of the deformation parameter $\varepsilon_{\mathrm{def}}$ for free and CNT-supported Pd_{561} clusters. At lower temperature before melting, $\varepsilon_{\mathrm{def}} \approx 1$ for both the free and CNT-supported Pd_{561} clusters. At higher temperatures near melting, some small jumps in $\varepsilon_{\mathrm{def}}$ are found for the free and CNT-supported Pd_{561} clusters, corresponding to the shape changes of the clusters upon melting, even the premelting phenomenon. At the melting points, sharp jumps are found for the free and CNT-supported Pd_{561} clusters, indicating the giant shape changes during the melting transition.

Figure 3(d) shows the temperature dependence of BOP W_6 for the free and CNT-supported Pd_{561} clusters. At lower temperature, the Mackay icosahedral structure is found for the free and CNT-supported Pd_{561} clusters, characterised by the standard value of W_6. However, at temperatures near the melting point, W_6 takes small jumps, indicating the structure evolution upon heating before melting. Then, giant jumps are found in W_6 during the melting temperatures. At the temperatures after melting, $W_6 \approx 0$ is found for both the free and CNT-supported Pd_{561} clusters, corresponding to the appearance of liquid phase after melting, characterised by the standard value of W_6.

The melting transitions of the free Pd_{55}, Pd_{147} and Pd_{309} clusters and those clusters encapsulated inside a (30, 30) CNT were analysed by means of the same four parameters. All melting points are summarised in Table 2. Melting temperatures are plotted as a function of $N^{-1/3}$ in Figure 4, where N represents the total number of Pd atoms in the free or CNT-supported Pd clusters. Linear decrease in cluster melting point with $N^{-1/3}$ is found for both the free and CNT-supported Pd clusters. This behaviour is in qualitative agreement with Pawlow's law [44].

It is clear from Table 2 and Figure 4 that the melting temperatures of the CNT-supported Pd clusters are lower than that of free Pd clusters, and the CNT support is thus responsible for this lowering. Previous results in the literature [45–47] related to a series of different clusters on an oxide substrate reveal that the substrate stabilises the clusters against melting. On the contrary, our results reveal

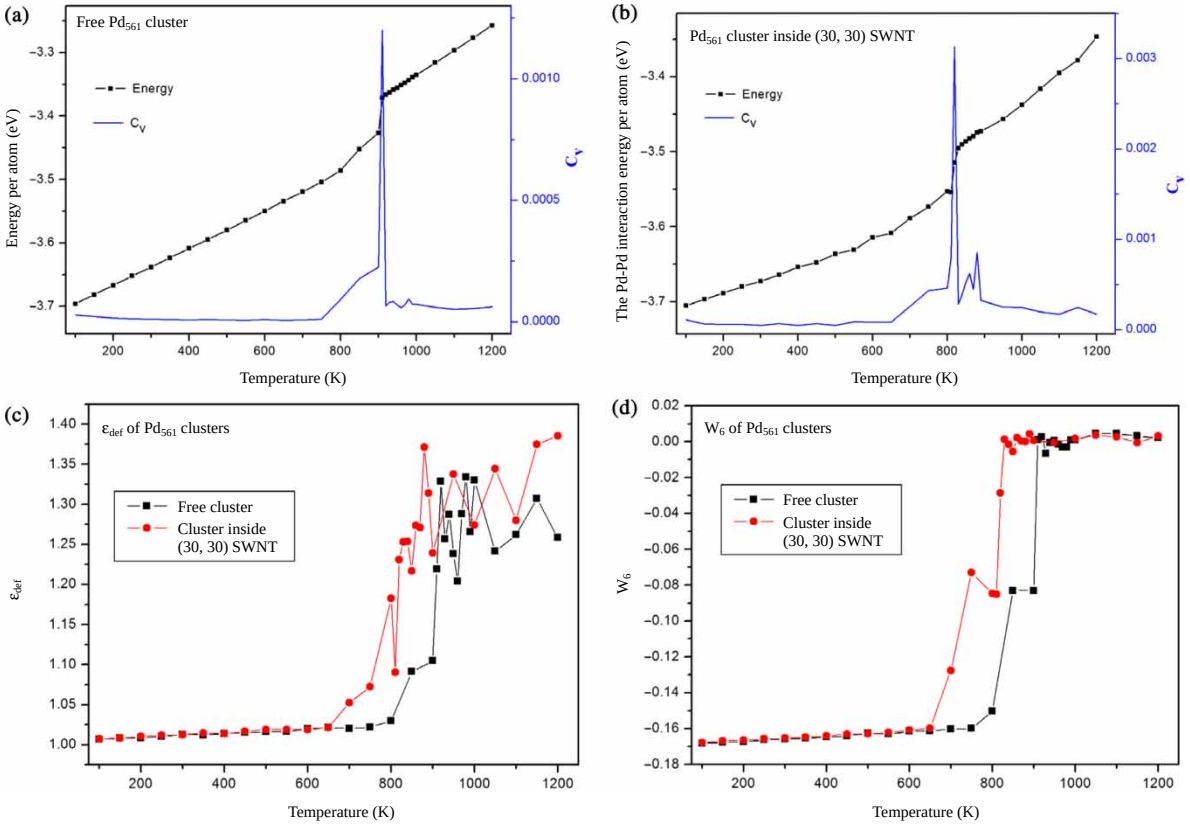

Figure 3. The caloric curve and the heat capacity C_v per atom of (a) the free Pd_{561} cluster and (b) the Pd_{561} cluster encapsulated inside the CNT. The temperature dependence of (c) the deformation parameter ε_{def} and (d) the BOP W_6 for the free (squares) and CNT-supported (circles) Pd_{561} clusters.

that even the Pd_{55} encapsulated inside a (30, 30) CNT could decrease the calculated melting point from 590 to 530 K, as shown in Table 2. The downward shift of the melting point may correlate with the reconstruction of the icosahedral Pd clusters at higher temperatures before melting. It is well known that the icosahedral structure is not the most favourable one for the system with cluster inside a CNT. The rearrangements and transformations of the clusters occur with the appearance of defects at higher temperatures before melting. Therefore, the sizes considered in this work are magic numbers (relatively more stable) for free clusters but not for supported clusters. This is an important factor, which could lead to the melting point depression of supported clusters.

Table 2. The melting points, T_m, of the free Pd_{55}, Pd_{147}, Pd_{309} and Pd_{561} clusters and those clusters encapsulated inside a (30, 30) CNT.

Clusters	Melting point of free clusters, T_m (free)	Melting point of clusters inside a (30, 30) SWNT, T_m (inside)	T_m (free) − T_m (inside)
Pd_{55} (K)	590	530	60
Pd_{147} (K)	740	670	70
Pd_{309} (K)	840	760	80
Pd_{561} (K)	910	820	90

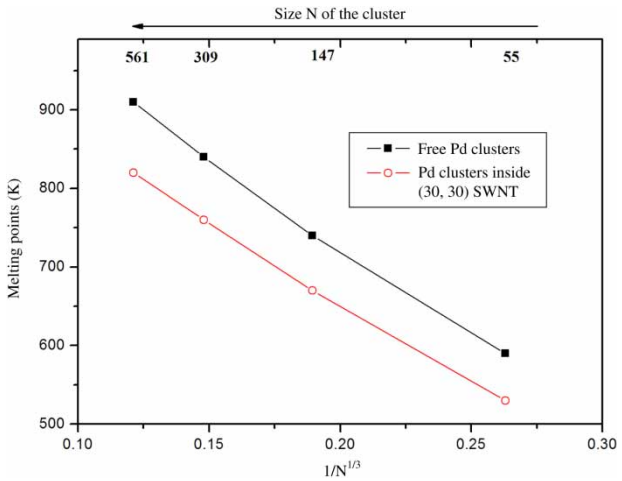

Figure 4. Melting temperatures changing with the inverse diameter of the cluster for the free (squares) and CNT-supported (circles) Pd clusters. A linear behaviour of the melting temperature with $N^{-1/3}$, the inverse diameter of the cluster, is found, which is in good qualitative agreement with Pawlow's law.

In general, the melting temperature of a cluster is influenced greatly by the distance in energy between its lowest energy structure and higher isomers [48]. Therefore, highly symmetric clusters as those found at geometric magic sizes (relatively more stable), which are likely to be well separated from higher isomers, usually melt at high temperature. In previous work, Mottet and Goniakowski [45], Mottet et al. [46] and Goniakowski et al. [47] compared the melting of supported magic clusters and free magic clusters in the same size range, and found that the supported clusters melt at much higher temperature. On the other hand, we found that the CNT substrate can destabilise the highly symmetric icosahedral cluster. It means that the icosahedral structure is not favourable on the curved surface of a CNT. This behaviour can considerably decrease the melting point.

Figure 5(a) shows the temperature dependence of the total Pd–Pd interaction energy per atom (i.e. the caloric curve) for the Pd_{147} cluster, encapsulated inside (15, 15), (20, 20), (25, 25), (30, 30) and (35, 35) CNTs. It is found in Figure 5(a) that the steps in the caloric curves occur at the same temperature for the Pd_{147} cluster, encapsulated inside different CNTs. The melting processes of the Pd_{147} cluster encapsulated inside different CNTs are also explored by the temperature dependence of the deformation parameter ε_{def} and the BOP W_6, as shown in Figure 5(b),(c), respectively. It is found in Figure 5(a)–(c) that the pronounced changes in the deformation parameter ε_{def} and the BOP W_6 are in good agreement with the step position in the caloric curves. All the melting indicators used thus converge to predict that the melting temperature of encapsulated Pd_{147} inside (15, 15), (20, 20), (25, 25), (30, 30) and (35, 35) CNTs is independent of the CNT diameter, which are all 670 K. This is clearly illustrated in Figure 6.

To understand the melting phenomenon, pair correlation functions $g(r)$ are employed, which are given by

$$g(r) = \frac{1}{n(n-1)} \sum_{i=1}^{n-1} \sum_{j>i}^{n} \delta(r - r_{ij}), \tag{4}$$

where n is the total number of the atoms in the cluster and r_{ij} is the distance between atoms i and j. $g(r)$ is calculated from the trajectories of the MD simulation after equilibrium, and the average first neighbour distance d is the modal position of the first peak. It is noticed that the

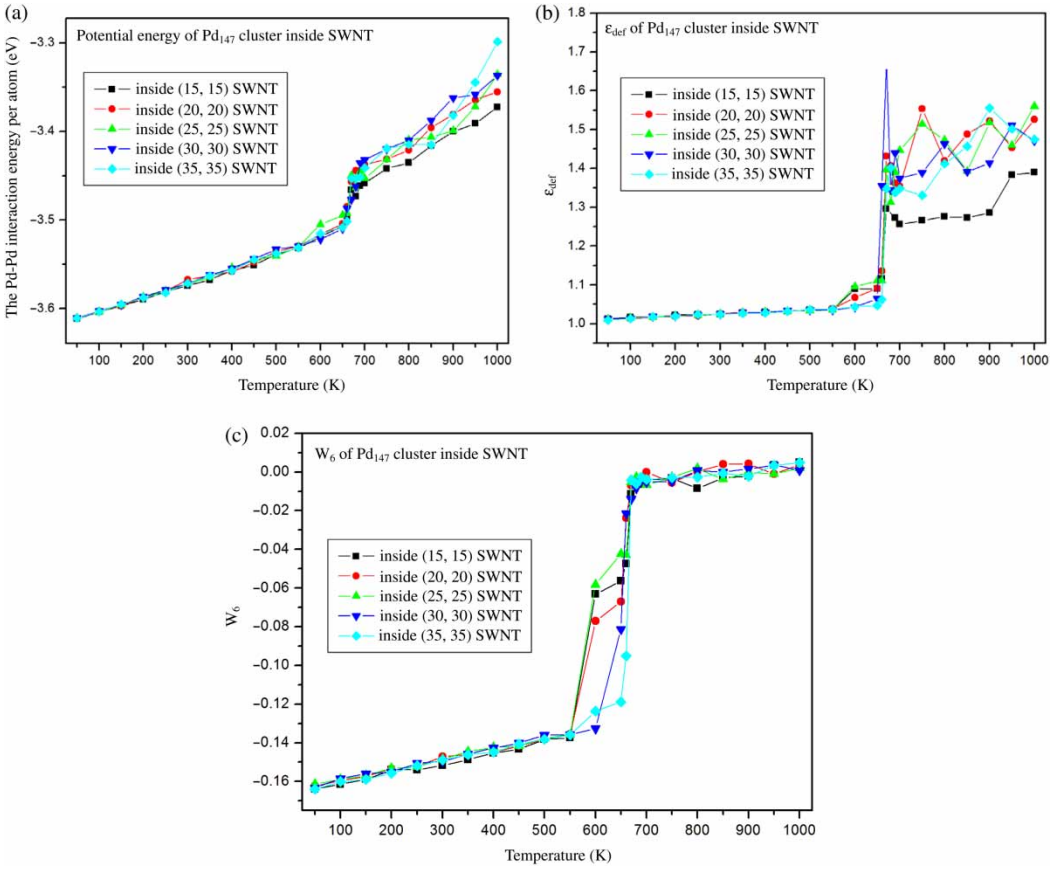

Figure 5. The temperature dependence of (a) the total Pd–Pd interaction energy per atom (i.e. the caloric curve), (b) the deformation parameter ε_{def} and (c) the BOP W_6 for the Pd_{147} cluster encapsulated inside (15, 15), (20, 20), (25, 25), (30, 30) and (35, 35) CNTs.

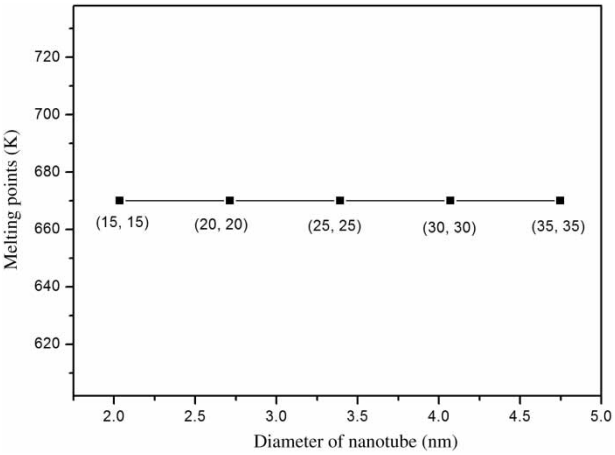

Figure 6. Melting temperatures as a function of the diameter of the CNT for the Pd_{147} cluster encapsulated inside (15, 15), (20, 20), (25, 25), (30, 30) and (35, 35) CNTs. Those melting points are all 670 K, meaning that the tube size has no effect on the melting of the Pd clusters inside the different CNTs.

properties of the second, third and fourth peaks in $g(r)$ are useful to characterise the crystalline state and phase transition. Figure 7(a), (b) shows the pair correlation functions of the free and (30, 30) CNT-supported Pd_{561} clusters, respectively, at several temperatures. As shown in Figure 7, the pair correlation functions display clearly four typical peaks at lower temperatures of 300 and 600 K, corresponding to the four first neighbour peaks in the fcc structure. It means that both the free and supported clusters are ordered. At 800 K, the second and more distant neighbour peaks are not so clear in the CNT-supported Pd_{561} cluster, which is the signature of the disordering of the fcc structure and may indicate that the cluster is in a state near or after melting. However, the free Pd_{561} cluster is still ordered at 800 K, identifying from the pair correlation functions. It means again that the melting temperatures of the CNT-supported Pd clusters should be lower than that of free Pd clusters. At 900 K, no clear second, third and fourth neighbour peaks are found for both the free and supported clusters, indicating that both the clusters are in a state near or after melting.

It is interesting to further explore the metal–tube interaction effect on the melting process. Here, we calculated the melting of the Pd_{147} cluster encapsulated inside (30, 30) CNTs using the DFT-Morse potential to model the Pd–C interaction (see definition in Section 2), in order to compare with the results using the VDW-LJ Pd–C potential. Figure 8(a) shows the temperature dependence of the total Pd–Pd interaction energy per atom (i.e. the caloric curve) for the Pd_{147} cluster encapsulated inside a (30, 30) CNT using both the DFT-Morse and VDW-LJ Pd–C potentials. The corresponding snapshots at 200, 400, 600, 700 and 900 K are also shown in Figure 8(b), (c) using the DFT-Morse and VDW-LJ

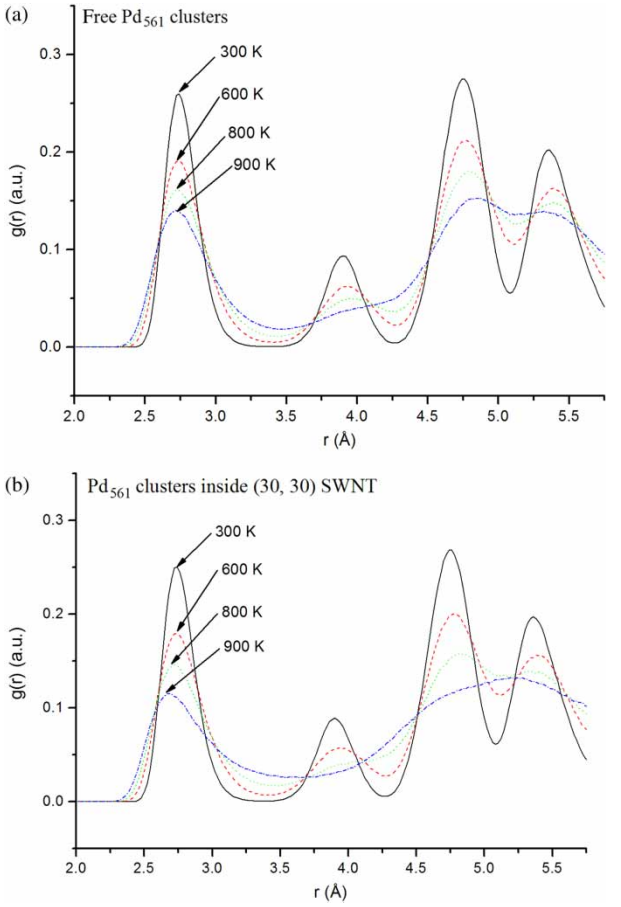

Figure 7. Pair correlation functions $g(r)$ of the (a) free and (b) (30, 30) CNT-supported Pd_{561} clusters at 300, 600, 800 and 900 K.

Pd–C potentials, respectively. At lower temperature (for example, 200 K), the icosahedral structure remains for both cases, as shown in Figure 8(a)–(c). Using the DFT-Morse Pd–C potential, a step jump is found at the temperature of 400 K corresponding to the structural transformation, and the icosahedral structure is transformed into the stacked one (see Figure 8(b)). Using the VDW-LJ Pd–C potential, the Pd_{147} cluster remains the icosahedral structure at the temperatures of 200, 400, 600 K before melting, and then a giant jump is found in the caloric curve at 700 K corresponding to the melting transition from solid to liquid. As shown in Figure 8(b), (c), the (30, 30) CNT has a giant deformation using the DFT-Morse Pd–C potential at even 200–900 K, but there is no deformation for the CNT using the VDW-LJ Pd–C potential at the same temperature. It may be due to the different Pd–C interaction. It means that the Pd–C potential representing the metal–tube interaction has a great effect on the melting of the Pd clusters inside the CNTs. In fact, the Pd–C interaction using the DFT-Morse Pd–C potential is about three to four times stronger than

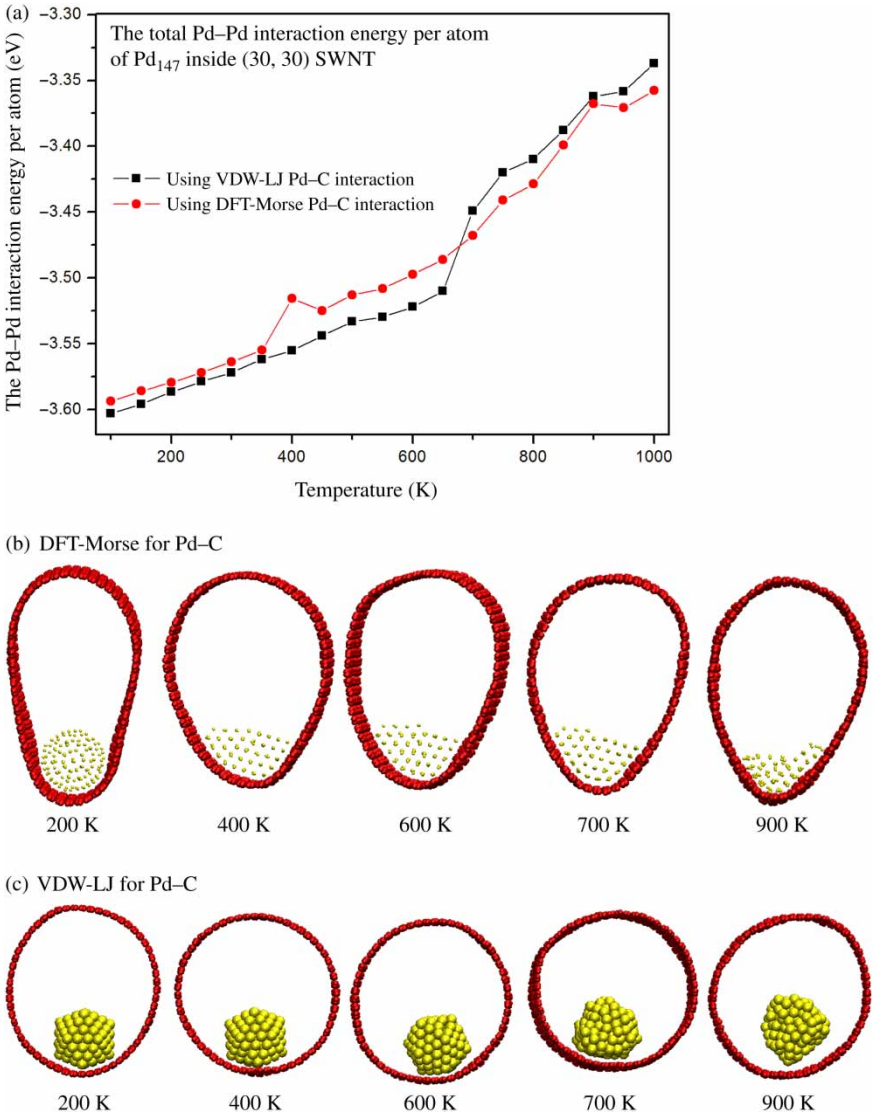

Figure 8. (a) The temperature dependence of the total Pd–Pd interaction energy per atom (i.e. the caloric curve) for the Pd_{147} cluster encapsulated inside a (30, 30) CNT using the DFT-Morse (circles) and VDW-LJ (squares) Pd–C potentials. The corresponding snapshots at 200, 400, 600, 700 and 900 K using the (b) DFT-Morse and (c) VDW-LJ Pd–C potentials.

that using the VDW-LJ Pd–C potential in this work (see the parameters in Section 2). The similar difference is also obtained by Acharya et al. [25] based on *ab initio* calculations.

4. Conclusions

To summarise, thermal behaviours of the icosahedral Pd clusters encapsulated in the CNTs were investigated by MD simulation, based on the TB-SMA for metal–metal interactions and Tersoff potential for the carbon–carbon interactions. The Pd–C interaction was modelled by both the weak VDW-LJ potential and the strong Morse-type (DFT-Morse) potential, which was fitted to first-principle calculations. The simulation results obtained using the VDW-LJ Pd–C potential indicate that the melting temperature of the CNT-contained Pd clusters is of linear behaviour with the inverse diameter of the clusters, which is in good agreement with Pawlow's law. It is also found that the melting temperature of the CNT-supported Pd cluster is much lower than that of free Pd cluster, due to reconstruction of the icosahedral clusters at higher temperatures before melting. Moreover, the Pd_{147} cluster encapsulated inside (15, 15), (20, 20), (25, 25), (30, 30) and (35, 35) CNTs is of the same melting temperature, indicating that the tube size has no effect on the melting of the Pd clusters inside different CNTs. Using the DFT-Morse Pd–C potential, deformation for the CNT and structural transformation from the

icosahedral to the stacked are found for the Pd cluster inside the CNTs. We believe that the results presented in this study will be helpful in applying and developing Pd clusters inside CNTs as sensors/catalysts.

Acknowledgements

We would like to thank Marc Hou for helpful comments and suggestions. This work was supported by the Foundation of Excellent Doctoral Dissertation of Beijing City (No. 200918).

References

[1] F. Baletto and R. Ferrando, *Structural properties of nanoclusters: Energetic, thermodynamic, and kinetic effects*, Rev. Mod. Phys. 77 (2005), pp. 371–423.

[2] R. Ferrando, J. Jellinek, and R.L. Johnston, *Nanoalloys: From theory to applications of alloy clusters and nanoparticles*, Chem. Rev. 108 (2008), pp. 845–910.

[3] N. Toshima and T. Yonezawa, *Bimetallic nanoparticles – Novel materials for chemical and physical applications*, New J. Chem. 22 (1998), pp. 1179–1201.

[4] S. Sun, C.B. Murray, D. Weller, L. Folks, and A. Moser, *Monodisperse FePt nanoparticles and ferromagnetic FePt nanocrystal superlattices*, Science 287 (2000), pp. 1989–1992.

[5] E. Cottancin, M. Gaudry, M. Pellarin, J. Lermé, L. Arnaud, J.R. Huntzinger, J.L. Vialle, M. Treilleux, P. Mélinon, J.-L. Rousset, and M. Broyer, *Optical properties of mixed clusters: Comparative study of Ni/Ag and Pt/Ag clusters*, Eur. Phys. J. D 24 (2003), pp. 111–114.

[6] F. Calvo and F. Spiegelmann, *Geometric size effects in the melting of sodium clusters*, Phys. Rev. Lett. 82 (1999), pp. 2270–2273.

[7] E. Cottancin, J. Lerme, M. Gaudry, M. Pellarin, J.L. Vialle, M. Broyer, B. Prevel, M. Treilleux, and P. Melinon, *Size effects in the optical properties of Au_nAg_n embedded clusters*, Phys. Rev. B 62 (2000), pp. 5179–5185.

[8] S. Liu, J. Zhu, Y. Mastai, I. Felner, and A. Gedanken, *Preparation and characteristics of carbon nanotubes filled with cobalt*, Chem. Mater. 12 (2000), pp. 2205–2211.

[9] C.K. Yang, J.J. Zhao, and J.P. Lu, *Magnetism of transition-metal/carbon-nanotube hybrid structures*, Phys. Rev. Lett. 90 (2003), p. 257203.

[10] Y.J. Kang, J. Choi, C.Y. Moon, and K.J. Chang, *Electronic and magnetic properties of single-wall carbon nanotubes filled with iron atoms*, Phys. Rev. B 71 (2005), p. 115441.

[11] M. Yang, Y. Yang, Y. Liu, G. Shen, and R. Yu, *Platinum nanoparticles-doped sol-gel/carbon nanotubes composite electrochemical sensors and biosensors*, Biosens. Bioelectron. 21 (2006), pp. 1125–1131.

[12] A.M. Zhang, J.L. Dong, Q.H. Xu, H.K. Rhee, and X.L. Li, *Palladium cluster filled in inner of carbon nanotubes and their catalytic properties in liquid phase benzene hydrogenation*, Catal. Today 93–95 (2004), pp. 347–352.

[13] Y. Lin, X. Cui, C. Yen, and C.M. Wai, *Platinum/carbon nanotube nanocomposite synthesized in supercritical fluid as electrocatalysts for low-temperature fuel cells*, J. Phys. Chem. B 109 (2005), pp. 14410–14415.

[14] J.-P. Tessonnier, L. Pesant, G. Ehret, M.J. Ledoux, and C. Pham-Huu, *Pd nanoparticles introduced inside multi-walled carbon nanotubes for selective hydrogenation of cinnamaldehyde into hydrocinnamaldehyde*, Appl. Catal. A 288 (2005), pp. 203–210.

[15] H.F. Cui, J.S. Ye, X. Liu, W.D. Zhang, and F.S. Sheu, *Pt–Pb alloy nanoparticle/carbon nanotube nanocomposite: A strong electrocatalyst for glucose oxidation*, Nanotechnology 17 (2006), pp. 2334–2339.

[16] Y. Lu, J. Li, J. Han, H.T. Ng, C. Binder, C. Partridge, and M. Meyyappan, *Room temperature methane detection using palladium loaded single-walled carbon nanotube sensors*, Chem. Phys. Lett. 391 (2004), pp. 344–348.

[17] S. Mubeen, T. Zhang, B. Yoo, M.A. Deshusses, and N.V. Myung, *Palladium nanoparticles decorated single-walled carbon nanotube hydrogen sensor*, J. Phys. Chem. C 111 (2007), pp. 6321–6327.

[18] Y. Sun, H.H. Wang, and M. Xia, *Single-walled carbon nanotubes modified with Pd nanoparticles: Unique building blocks for high-performance, flexible hydrogen sensors*, J. Phys. Chem. C 112 (2008), pp. 1250–1259.

[19] D. Cheng, W. Wang, and S. Huang, *Thermal evolution of a platinum cluster encapsulated in carbon nanotubes*, J. Phys. Chem. C 111 (2007), pp. 1631–1637.

[20] S. Arcidiacono, J.H. Walther, D. Poulikakos, D. Passerone, and P. Koumoutsakos, *Solidification of gold nanoparticles in carbon nanotubes*, Phys. Rev. Lett. 94 (2005), p. 105502.

[21] B.H. Morrow and A. Striolo, *Morphology and diffusion mechanism of platinum nanoparticles on carbon nanotube bundles*, J. Phys. Chem. C 111 (2007), pp. 17905–17913.

[22] B.H. Morrow and A. Striolo, *Platinum nanoparticles on carbonaceous materials: The effect of support geometry on nanoparticle mobility, morphology, and melting*, Nanotechnology 19 (2008), p. 195711.

[23] V.R. Bhethanabotla and W.A. Steele, *Computer-simulation study of melting in dense oxygen layers on graphite*, Phys. Rev. B 41 (1990), p. 9480.

[24] P.M. Agrawal, B.M. Rice, and D.L. Thompson, *Predicting trends in rate parameters for self-diffusion on FCC metal surfaces*, Surf. Sci. 515 (2002), pp. 21–35.

[25] C.K. Acharya, D.I. Sullivan, and C.H. Turner, *Characterizing the interaction of Pt and PtRu clusters with boron-doped, nitrogen-doped, and activated carbon: Density functional theory calculations and parameterization*, J. Phys. Chem. C 112 (2008), pp. 13607–13622.

[26] B.H. Morrow and A. Striolo, *Assessing how metal–carbon interactions affect the structure of supported platinum nanoparticles*, Mol. Sim. 35 (2009), pp. 795–803.

[27] G. Chen and Y. Kawazoe, *Interaction between a single Pt atom and a carbon nanotube studied by density functional theory*, Phys. Rev. B 73 (2006), p. 125410.

[28] W. Smith and T.R. Forester, *DL_POLY_2.0: A general-purpose parallel molecular dynamics simulation package*, J. Mol. Graphics 14 (1996), pp. 136–141.

[29] H.J.C. Berendsen, J.P.M. Postma, W.F. van Gunsteren, A. DiNola, and J.R. Haak, *Molecular dynamics with coupling to an external bath*, J Chem. Phys. 81 (1984), pp. 3684–3690.

[30] F. Cleri and V. Rosato, *Tight-binding potentials for transition metals and alloys*, Phys. Rev. B 48 (1993), pp. 22–33.

[31] J. Tersoff, *Empirical interatomic potential for carbon, with applications to amorphous carbon*, Phys. Rev. Lett. 61 (1988), pp. 2879–2882.

[32] W.Y. Choi, J.W. Kang, and H.J. Hwang, *Structures of ultrathin copper nanowires encapsulated in carbon nanotubes*, Phys. Rev. B 68 (2003), p. 193405.

[33] H.J. Hwang, O.-K. Kwon, and J.W. Kang, *Copper nanocluster diffusion in carbon nanotube*, Solid State Commun. 129 (2004), pp. 687–690.

[34] S.K.R.S. Sankaranarayanan, V.R. Bhethanabotla, and B. Joseph, *Molecular dynamics simulations of the structural and dynamic properties of graphite-supported bimetallic transition metal clusters*, Phys. Rev. B 72 (2005), p. 195405.

[35] G.E. Scuseria, M.A. Robb, J.R. Cheeseman, J.A. Montgomery, Jr, T. Vreven, K.N. Kudin, J.C. Burant, J.M. Millam, S.S. Iyengar, J. Tomasi, V. Barone, B. Mennucci, M. Cossi, G. Scalmani, N. Rega, G.A. Petersson, H. Nakatsuji, M. Hada, M. Ehara, K. Toyota, R. Fukuda, J. Hasegawa, M. Ishida, T. Nakajima, Y. Honda, O. Kitao, H. Nakai, M. Klene, X. Li, J.E. Knox, H.P. Hratchian, J.B. Cross, V. Bakken, C. Adamo, J. Jaramillo, R. Gomperts, R.E. Stratmann, O. Yazyev, A.J. Austin, R. Cammi, C. Pomelli, J.W. Ochterski, P.Y. Ayala, K. Morokuma, G.A. Voth, P. Salvador, J.J. Dannenberg, V.G. Zakrzewski, S. Dapprich, A.D. Daniels, M.C. Strain, O. Farkas, D.K. Malick, A.D. Rabuck, K. Raghavachari, J.B. Foresman, J.V. Ortiz, Q. Cui, A.G. Baboul, S. Clifford, J. Cioslowski, B.B. Stefanov, G. Liu, A. Liashenko, P. Piskorz, I. Komaromi, R.L. Martin, D.J. Fox, T. Keith, M.A. Al-Laham, C.Y. Peng, A. Nanayakkara, M. Challacombe, P.M.W. Gill,

B. Johnson, W. Chen, M.W. Wong, C. Gonzalez, and J.A. Pople, *GAUSSIAN 03, Revision B.02*, Gaussian, Inc., Wallingford, CT, 2004.

[36] M.K. Kostov, E.E. Santiso, A.M. George, K.E. Gubbins, and M.B. Nardelli, *Dissociation of water on defective carbon substrates*, Phys. Rev. Lett. 95 (2005), p. 136105.

[37] G. Mpourmpakis, G.E. Froudakis, G.P. Lithoxoos, and J. Samios, *SiC nanotubes: A novel material for hydrogen storage*, Nano Lett. 6 (2006), pp. 1581–1583.

[38] J. Lan, D. Cheng, D. Cao, and W. Wang, *Silicon nanotube as a promising candidate for hydrogen storage: From the first principle calculations to grand canonical Monte Carlo simulations*, J. Phys. Chem. C 112 (2008), pp. 5598–5604.

[39] J.P. Perdew and Y. Wang, *Accurate and simple analytic representation of the electron-gas correlation energy*, Phys. Rev. B 45 (1992), pp. 13244–13249.

[40] S. Chacko, D.G. Kanhere, and S.A. Blundell, *First principles calculations of melting temperatures for free Na clusters*, Phys. Rev. B 71 (2005), p. 155407.

[41] P.J. Steinhardt, D.R. Nelson, and M. Ronchetti, *Bond-orientational order in liquids and glasses*, Phys. Rev. B 28 (1983), pp. 784–805.

[42] C.L. Kuo and P. Clancy, *Melting and freezing characteristics and structural properties of supported and unsupported gold nanoclusters*, J. Phys. Chem. B 109 (2005), pp. 13743–13754.

[43] D. Cheng and D. Cao, *Structural transition and melting of onion-ring Pd–Pt bimetallic clusters*, Chem. Phys. Lett. 461 (2008), pp. 71–76.

[44] P. Pawlow, *Über die Abhängigkeit des Schmelzpunktes von der Oberflächenenergie eines festen Körpers*, Z. Phys. Chem. (Leipzig) 65 (1909), pp. 1–35.

[45] C. Mottet and J. Goniakowski, *Melting and freezing of Pd nanoclusters: Effect of the MgO(1 0 0) substrate*, Surf. Sci. 566–568 (2004), pp. 443–450.

[46] C. Mottet, J. Goniakowski, F. Baletto, R. Ferrando, and G. Treglia, *Modeling free and supported metallic nanoclusters: Structure and dynamics*, Phase Transit. 77 (2004), pp. 101–113.

[47] J. Goniakowski, C. Mottet, and C. Noguera, *Non-reactive metal/oxide interfaces: From model calculations towards realistic simulations*, Phys. Stat. Sol. (b) 243 (2006), pp. 2516–2532.

[48] Z. Kuntov, G. Rossi, and R. Ferrando, *Melting of core-shell Ag–Ni and Ag–Co nanoclusters studied via molecular dynamics simulations*, Phys. Rev. B 77 (2008), p. 205431.